AD-A162 531

X-Ray Microbursts and VLF Chorus

Prepared by

J. L. ROEDER
Space Sciences Laboratory
Laboratory Operations
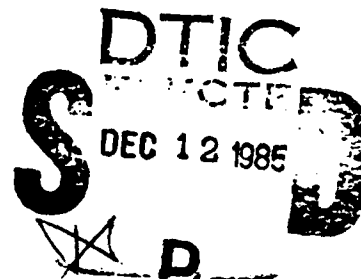The Aerospace Corporation
El Segundo, CA 90245

and

J. R. BENBROOK, E. A. BERING, W. R. SHELDON, and E. G. STANSBERRY
Department of Physics
University of Houston
Houston, TX 77004

30 September 1985

DTIC

DEC 12 1985

APPROVED FOR PUBLIC RELEASE;
DISTRIBUTION UNLIMITED

Prepared for

SPACE DIVISION
AIR FORCE SYSTEMS COMMAND
Los Angeles Air Force Station
P.O. Box 92960, Worldway Postal Center
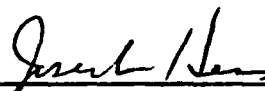Los Angeles, CA 90009-2960

85 12 12 085

This report was submitted by The Aerospace Corporation, El Segundo, CA 90245, under Contract No. F04701-83-C-0084 with the Space Division, P.O. Box 92960, Worldway Postal Center, Los Angeles, CA 90009-2960. It was reviewed and approved for The Aerospace Corporation by H. R. Rugge, Director, Space Sciences Laboratory. Captain Douglas R. Case, YCM, was the project officer for the Mission-Oriented Investigation and Experimentation (MOIE) program.

This report has been reviewed by the Public Affairs Office (PAS) and is releasable to the National Technical Information Service (NTIS). At NTIS, it will be available to the general public, including foreign nationals.

This technical report has been reviewed and is approved for publication. Publication of this report does not constitute Air Force approval of the report's findings or conclusions. It is published only for the exchange and stimulation of ideas.

DOUGLAS R. CASE, Capt, USAF
MOIE Project Officer
SD/YCM

JOSEPH HESS, GM-15
Director, AFSTC West Coast Office
AFSTC/WCO OL-AB

REPORT DOCUMENTATION PAGE		READ INSTRUCTIONS BEFORE COMPLETING FORM
1. REPORT NUMBER SD-TR-85-71	2. GOVT ACCESSION NO.	3. RECIPIENT'S CATALOG NUMBER
4. TITLE *(and Subtitle)* X-Ray Microbursts and VLF Chorus		5. TYPE OF REPORT & PERIOD COVERED
		6. PERFORMING ORG. REPORT NUMBER TR-0084A(5940-06)-4
7. AUTHOR(*s*) J. L. Roeder, J. R. Benbrook, E. A. Bering, W. R. Sheldon, and E. G. Stansberry		8. CONTRACT OR GRANT NUMBER(*s*) F04701-83-C-0084
9. PERFORMING ORGANIZATION NAME AND ADDRESS The Aerospace Corporation El Segundo, CA 90245		10. PROGRAM ELEMENT, PROJECT, TASK AREA & WORK UNIT NUMBERS
11. CONTROLLING OFFICE NAME AND ADDRESS Space Division Los Angeles Air Force Station Los Angeles, CA 90009-2960		12. REPORT DATE 30 September 1985
		13. NUMBER OF PAGES 24
14. MONITORING AGENCY NAME & ADDRESS*(if different from Controlling Office)*		15. SECURITY CLASS. *(of this report)* Unclassified
		15a. DECLASSIFICATION/DOWNGRADING SCHEDULE

16. DISTRIBUTION STATEMENT *(of this Report)*

Approved for public release; distribution unlimited.

17. DISTRIBUTION STATEMENT *(of the abstract entered in Block 20, if different from Report)*

18. SUPPLEMENTARY NOTES

19. KEY WORDS *(Continue on reverse side if necessary and identify by block number)*

Microburst, VLF Chorus, Wave-particle Interaction

20. ABSTRACT *(Continue on reverse side if necessary and identify by block number)*

On January 4, 1978, at 1140 UT, a Super Arcas sounding rocket was launched from Siple Station, Antarctica (L = 4.2, 76°S, 84°W) during a geomagnetically disturbed period ($K_p = 6-$) with intense X-ray and VLF chorus activity. The parachuted payload observed an intense microburst precipitation event of 10 minute duration. These data have been correlated with measurements of VLF chorus by receivers on the ground at both Siple and its

DD ^{FORM} 1473
FACSIMILE

19. KEY WORDS (Continued)

20. ABSTRACT (Continued)

magnetic conjugate point, Roberval, Quebec. Detailed one-to-one corre-
spondence between the microbursts and the chorus was not a consistent
feature of the data. Time series analysis of the data did indicate a
significant correlation between the Siple X-ray precipitation and the
Roberval VLF waves with an arrival time delay of 0.1 ⊕ 0.3 seconds.

CONTENTS

1

FIGURES

Accesion For

NTIS CRA&I		☑
DTIC TAB		☐
Unannounced		☐
Justification		

By

Distribution /

Availability

Dist	Avail and / or Special
A-1	

I. INTRODUCTION

A form of electron precipitation known as microbursts is a common feature of the morning sector of the magnetosphere. Originally seen in balloon X-ray bremsstrahlung measurements (Anderson and Milton, 1964), microbursts are transient enhancements of duration ~ 0.2 second. The scale size of microbursts is small (radius < 100 km at ionospheric altitudes). Parks (1975 and 1978) reviewed these and other details of microburst precipitation. Attempts have been made to locate the source region of the bursts from the dispersion of the arrival time of the particles as a function of energy. They produced source locations along with field lines from the equatorial plane to 1 R_E altitude (Anderson and Milton, 1964; Lampton, 1967; Haugstad and Pytte, 1977). Microbursts are observed to occur most frequently at the latitudes and local times of maximum VLF chorus activity (Oliven et al., 1968). A statistical study of precipitating electrons and VLF waves observed via satellite concluded that electron microbursts were always accompanied by chorus emissions, but that a one-to-one correspondence between the particle and wave features did not exist (Oliven and Gurnett, 1968). This lack of detailed correlations between chorus emissions and electron precipitation is a significant and pervasive feature of microburst events that is not addressed by current theoretical treatment.

Rosenberg et al. (1971) presented simultaneous balloon X-ray and ground VLF data acquired at Siple Station, Antarctica, that showed a one-to-one correspondence between microbursts and VLF emissions for a limited segment of data. Evidence for the triggering of the emissions by lightning-generated whistlers was found in spectrograms of the VLF data. Foster and Rosenberg (1976) reported an extensive analysis of those data and concluded that cyclotron resonance in the equatorial plane was responsible for the correlation. The model used to explain the correlation is illustrated schematically in Figure 1a. Whistler-mode waves generated by lightning in the northern hemisphere propagate southward in a duct, and northward-bound electrons resonate with the waves in the interaction region near the equator. Wave growth and
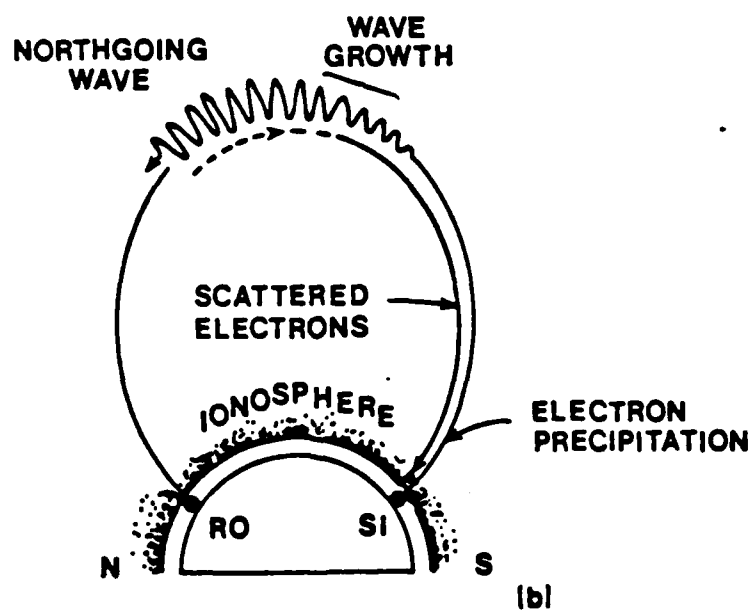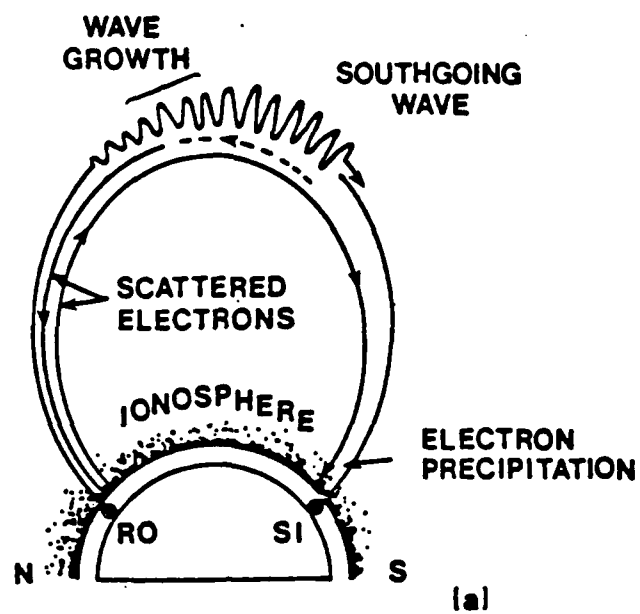
Fig. 1. Schematics of proposed wave-particle interaction mechanisms [taken from Helliwell et al. (1980)].

emission triggering occur as the resonant electrons scatter to lower pitch angles. The asymmetry in mirror heights between the Roberval and Siple ends of the field line allows a fraction of the scattered electrons to be reflected over Roberval and be precipitated at Siple. This model is consistent with the observed time lag of ~ 0.2 seconds between the reception of a VLF burst at Siple Station and the detection of the X-ray burst at Siple Station. The relationship of the microburst-chorus event to a complex substorm in progress at that time was reported separately (Carpenter et al., 1975; Foster et al., 1976).

A similar interaction, depicted in Figure 1b, was employed by Helliwell et al. (1980) to explain correlated optical observations at Siple with VLF-wave features at Siple and Roberval. In this case the whistler and its associated emissions were reflected by the ionosphere at Siple. The waves were then amplified and triggered new emissions as they traveled back northward across the equator. Thus, southward-going electrons were scattered directly into the Siple loss cone.

A preliminary report of two other instances of this type of wave-particle interaction was given by Rosenberg et al. (1978). The experimental observations included X-ray and VLF-wave measurements from a balloon near Roberval, and VLF data from a ground receiver at Siple. A detailed study of those events by Rosenberg et al. (1981) concluded that the interactions were similar to those of Foster and Rosenberg (1976). However, the X-ray precipitation at Siple was not measured during the events. Rosenberg et al. (1981) also presented evidence of a spatial separation along the field line of the wave-growth and pitch-angle scattering regions. Furthermore, to achieve agreement between the theoretical and observed time lags between VLF and X-ray bursts, they had to assume a non-negligible time delay in the pitch angle scattering process itself (~ 70 - 80 milliseconds).

Inan and collaborators have published a number of papers recently that address the problem of calculating the energy spectrum and the time profile of the observed precipitating electrons for an assumed time profile for the VLF wave (see, for example, Inan et al., 1982; Chang and Inan, 1983; Inan et al.,

1984). Specifying the time profile of the VLF wave permits the region of wave amplification to be located at a different place along the magnetic field line from the region where pitch-angle scattering moves electrons into the loss cone. Amplification can then occur through interaction of the VLF wave with electrons of larger pitch angle which are not scattered into the loss cone. The amplified wave subsequently interacts with other energetic electrons whose pitch angles are near the loss cone and induces precipitation. The additional freedom in this model, along with suitable choices of ambient magnetospheric conditions, has improved agreement between observation and calculation with regard to relative arrival times of chorus emissions and electron precipitation. The calculated X-ray pulse shapes produced by the electrons are still less than satisfactory with regard to rise time, duration, and spectrum, however.

In this report, data from a Super Arcas sounding rocket experiment flown from Siple Station, Antarctica, on January 4, 1978, and from a VLF receiver located at Siple and its magnetically conjugate point, Roberval, Quebec, are presented and compared. An extensive time series analysis of the data has been conducted to determine the nature of the correlations between the data sets.

The X-ray and electron precipitation measurements during the January 4, 1978, event were made with a University of Houston rocket payload that was boosted to an altitude of 80 km by a Super Arcas sounding rocket. At apogee the payload was deployed on a 16.5 foot diameter disc-gap-band Mylar parachute. It then drifted down slowly, providing approximately 12 minutes of data above an altitude of 30 km. The primary detectors on the payload were a NaI scintillator which measured X-rays above 5 keV and a Geiger counter sensitive to electrons above 55 keV. Detailed descriptions of these payloads have been published previously (Roeder et al., 1980; Bering et al., 1980; Benbrook et al., 1983).

8

II. EXPERIMENTAL RESULTS

Plots of the scintillation integral energy data and the Geiger counter data versus Universal Time for the entire duration of the microburst event are displayed in Figure 2. All the data shown are one second averages in units of flux (counts s^{-1} cm^{-2} sr^{-1}). Scales marked in counting rate (counts s^{-1}) are also given on the right side of all panels. Four panels show the integral fluxes obtained from the scintillation counter at energies > 5 keV, > 15 keV, > 30 keV and > 50 keV.

The payload altitude in kilometers is given at the top of the figure. In the first part of the event, groups of X-ray microbursts were observed every 10 to 20 seconds, with four to six bursts per group. The average time between individual bursts was 0.6 seconds. The mean width of the X-ray bursts during the event was 0.2 seconds. At 1153:40 UT the character of the time variations of the X-ray flux changed to a continuously bursting mode, with a period of approximately 0.5 second. This active part of the event slowly decayed to background with increasing time, an effect that is due in part to the increasing X-ray attenuation as the detector sank in the atmosphere.

In Figure 3 both X-ray and VLF data are presented for a thirty-second interval of data starting at 1148 UT. The top four panels present the X-ray data from the rocket in 0.2 second averages, in units of flux and counting rate. The bottom panels display the VLF data taken at Siple and Roberval. The VLF data from each of the two locations are shown in two formats: a grey scale spectrogram and integrated intensity of the VLF in two frequency intervals. The ordinates of the spectrograms are wave frequency, plotted linearly from zero to 5 kHz; the time resolution of the spectrograms is approximately 0.01 seconds; and the darkness of the pattern is proportional to the power of the signal. The VLF integrated intensities were computed in each case from digital spectra of the broadband waveforms. In this figure the frequency bands chosen were broad enough to cover all the observed emissions: 1 - 4.5 kHz for the Siple data, and 1.5 - 4.5 kHz for the Roberval VLF. The intensity of each of the VLF signals is displayed as 0.1 second averages in Figure 3.

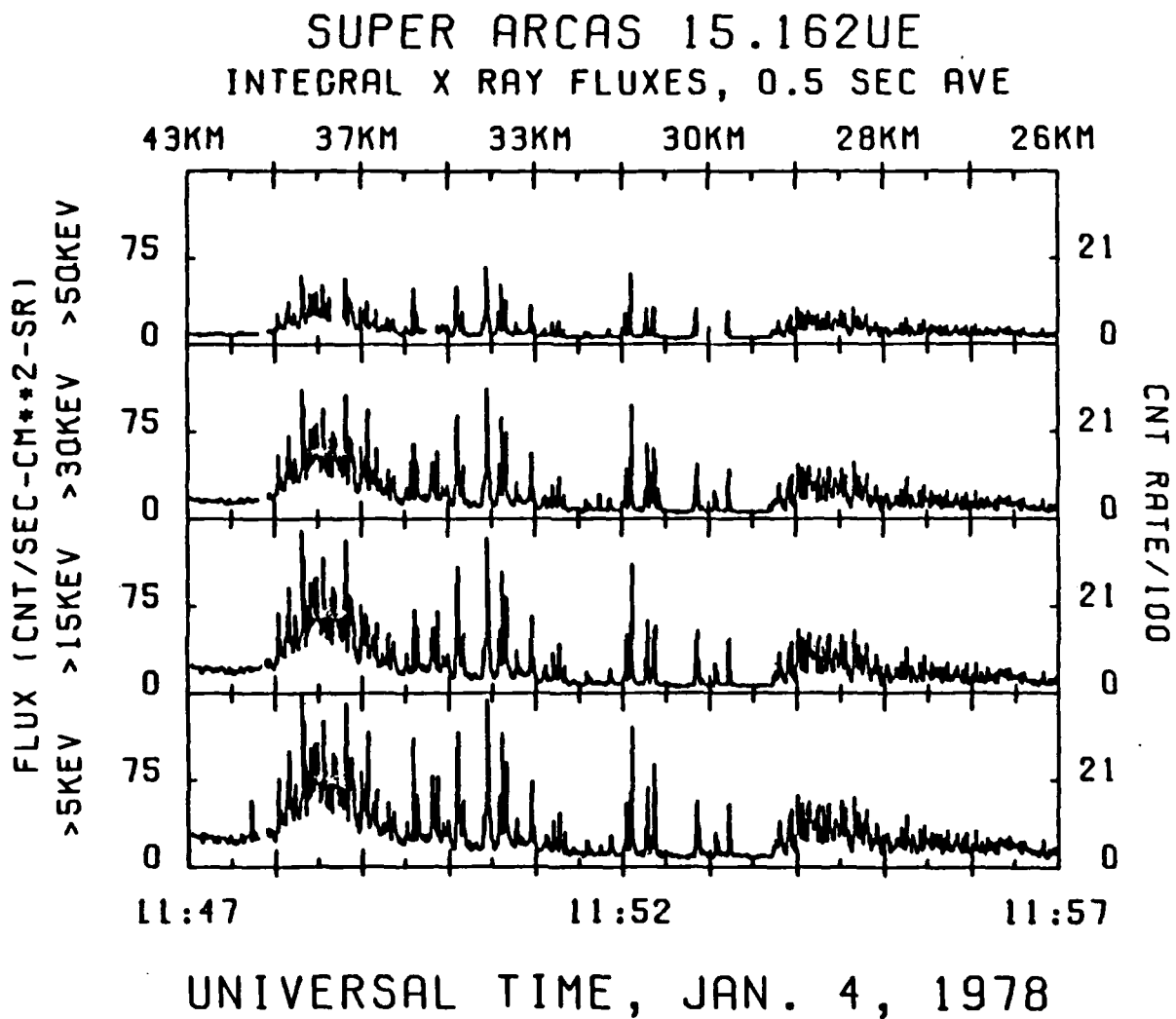Fig. 2. Integral X-ray fluxes during the microburst precipitation event between 1147 UT and 1157 UT. The payload altitude is marked on the top scale.

SUPER ARCAS 15.162UE X-RAYS,0.1 SEC AVE
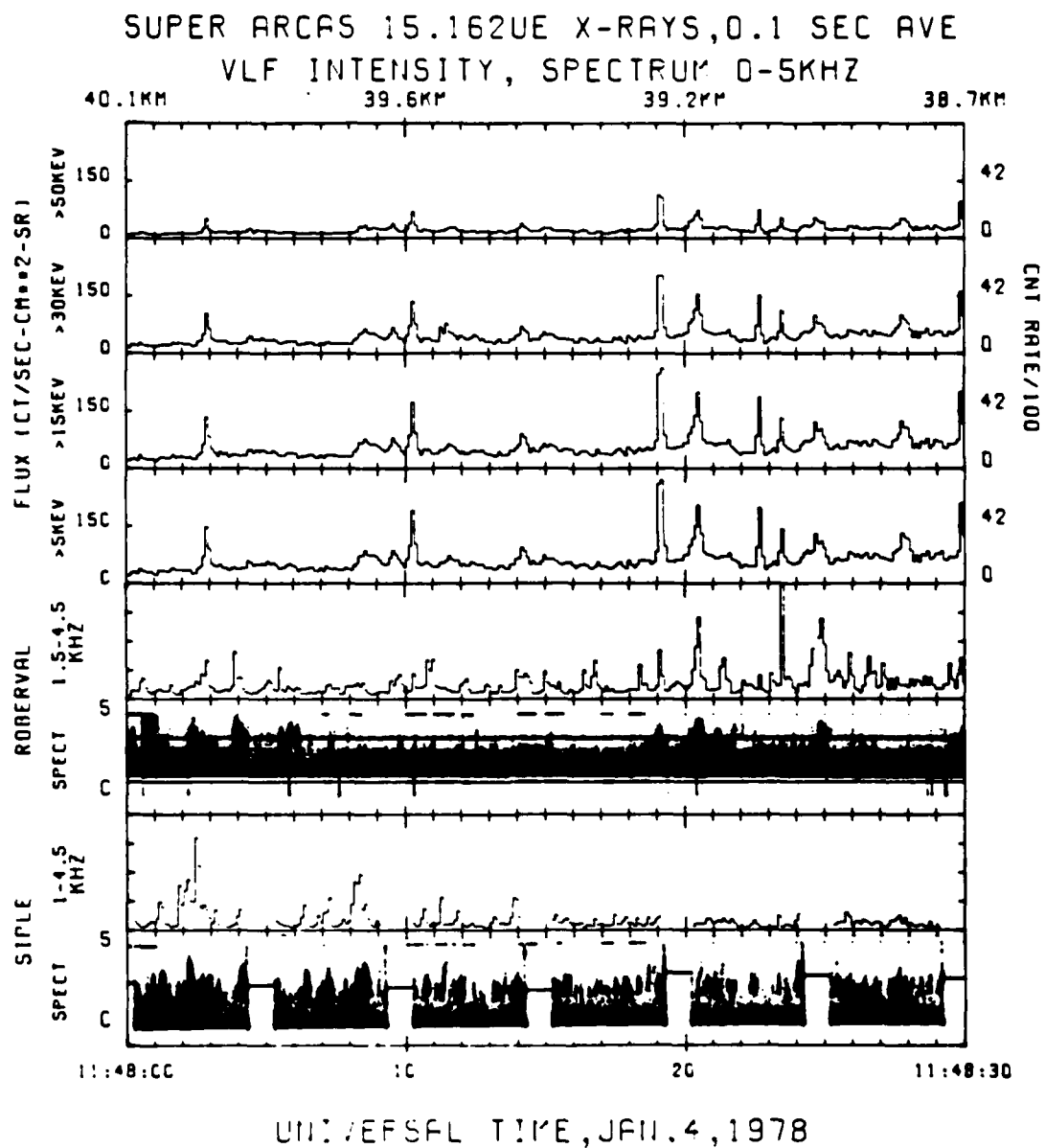VLF INTENSITY, SPECTRUM 0-5KHZ

Fig. 3. X-ray fluxes and VLF wave measurements for 1148:00 - 1148:30 UT. The waves at Siple and Roberval are each presented in frequency-time spectrograms and total intensity plots.

11

The one-second pulses evident in the Siple VLF spectrogram are the signature of the Stanford University VLF transmitter experiment at Siple. During the rocket flight the transmitter was operating continuously, using a program that consisted of a thirty second cycle of the second-wide pulses every five seconds. To simplify the graph of the Siple VLF intensity in Figure 3 the data were edited to remove the transmitter pulses. The Roberval VLF data showed no trace of the signal transmitted from Siple. The ordinates of the VLF intensity panels are in arbitrary units, since no absolute calibration for the VLF data was performed.

The data shown in Figure 3 exhibit the large variety of features that were typical of this flight. The microbursts in the X-ray data were quite pronounced, being a factor of 6 to 8 above the background. The widths of the bursts were highly variable, ranging from one second to one-tenth of a second. The grouped characteristics of the bursts can also be noted in Figure 3. The VLF data are much more complex for several reasons. The range of the VLF receiver is approximately ten times the viewing range of the X-ray detector, so that many of the received emissions may be unrelated to the local X-ray precipitation. The emissions observed cover a wide range of frequencies that are all averaged together in the intensity graph. There is no obvious one-to-one correspondence between X-ray bursts and VLF emissions during this interval, but there is a noticeable tendency for a microburst at Siple and an emission at Roberval to occur almost simultaneously. For example, the X-ray bursts at 1148:19 and 1148:20.5 UT have corresponding radio emissions in the Roberval VLF intensity. However, there are many instances of an X-ray microburst that has no matching VLF emission and, of the converse, an emission without a microburst.

. The amount of correlation between the X-ray and the VLF observations was extremely variable throughout the interval studied. At times when there was some similarity between the structure of the X-ray data and the VLF intensity, the apparent time delay between the arrival of the X-ray burst at Siple and the VLF emission at Roberval was small (magnitude less than 0.2 s), except in a few isolated cases. The microburst at 1149:07.2 UT in Figure 4 was the most intense enhancement observed by 15.162 UE during the second pulsation interval
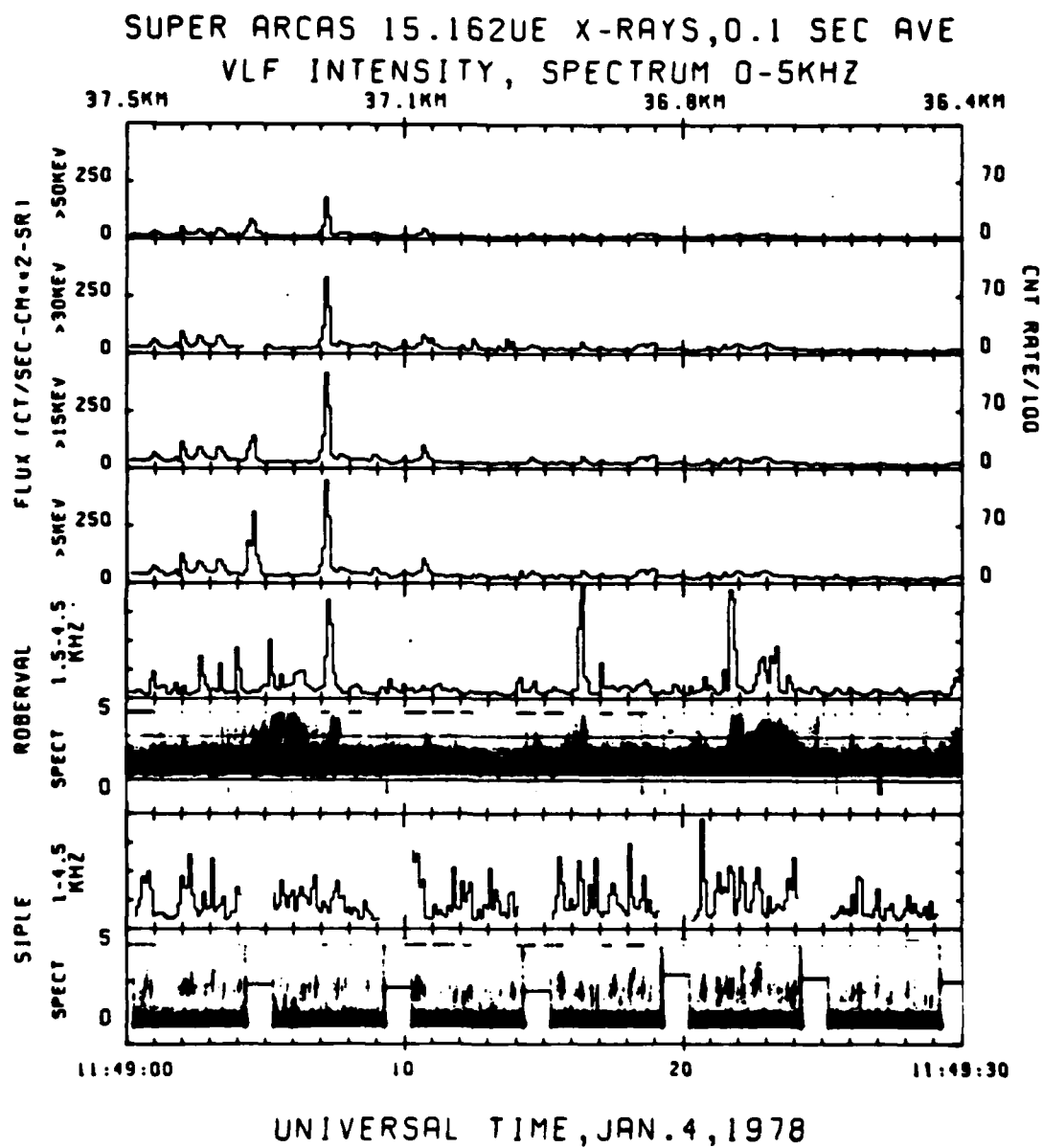
12

SUPER ARCAS 15.162UE X-RAYS,0.1 SEC AVE
VLF INTENSITY, SPECTRUM 0-5KHZ

UNIVERSAL TIME,JAN.4,1978

Fig. 4.   X-ray fluxes and VLF wave data for 1149:00 - 1149:30 UT.

13

beginning at 1147:50 UT. With a peak flux of 450 counts s^{-1} cm^{-2} sr^{-1} for approximately 0.2 s duration, it represents about 2700 photons detected by the instrument. This rate is over twenty times more intense than any X-ray bursts at this location reported by Foster and Rosenberg (1976) or Rosenberg et al. (1981).

At approximately 1153:40 UT the character of the X-ray and VLF data changed markedly after a relatively quiet thirty-second period. The variation in the X-ray and VLF intensity increased as the event acquired a continuous nature, in contrast to the previous discrete group of emissions and microbursts. The further evolution of the data can be noted in Figure 5. The X-ray flux and the VLF intensity were highly correlated at this time with a very small time delay, probably less than 0.2 s. After the period shown by Figure 5, the amplitude of the X-ray flux variations slowly decreased, probably due to increasing X-ray attenuation as the payload sank in the atmosphere.
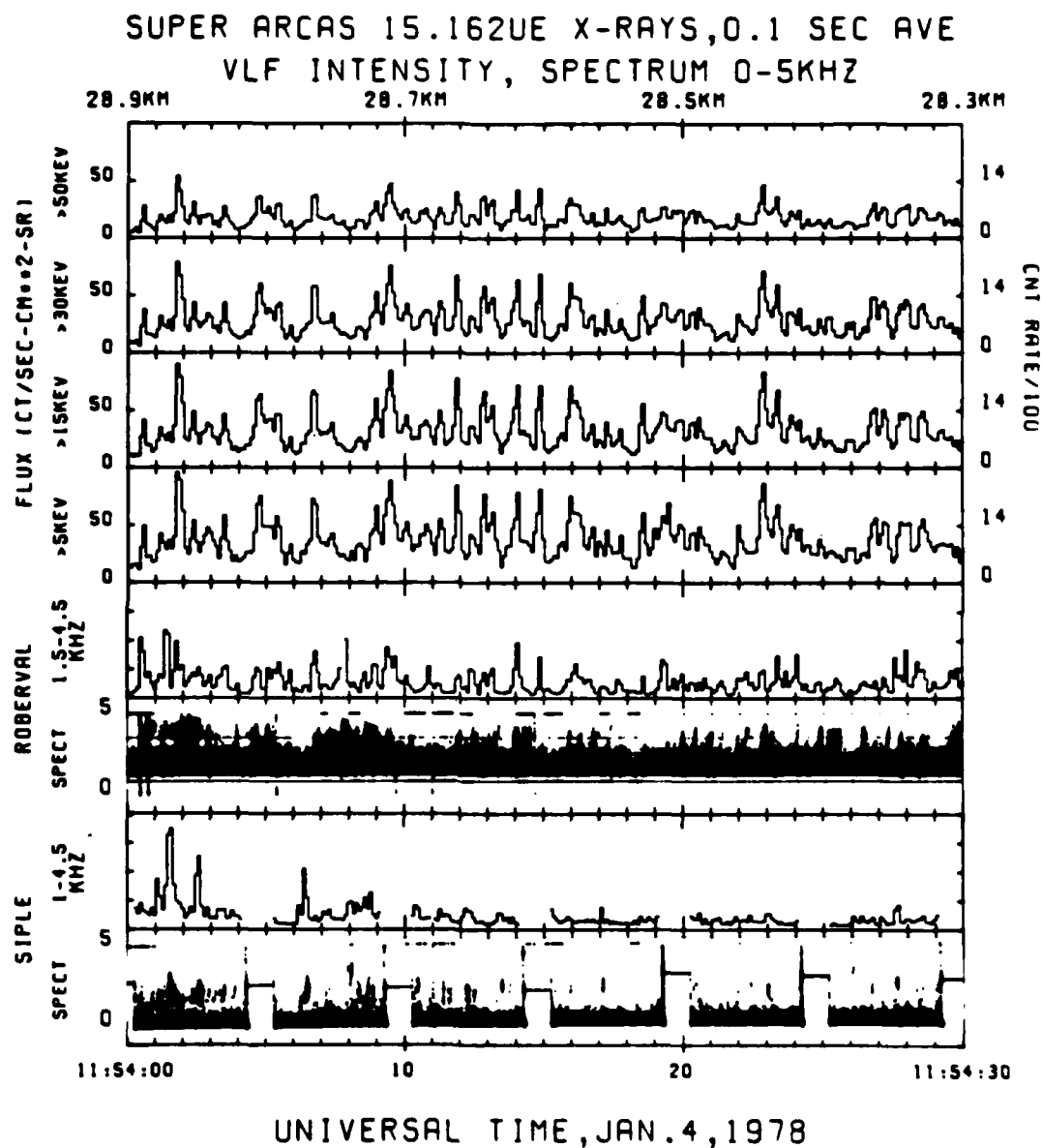
14

SUPER ARCAS 15.162UE X-RAYS,0.1 SEC AVE
VLF INTENSITY, SPECTRUM 0-5KHZ

UNIVERSAL TIME, JAN.4,1978

Fig. 5. X-ray fluxes and VLF wave data for 1154:00 - 1154:30 UT.

15

III. TIME SERIES ANALYSIS OF THE X-RAY AND VLF DATA

An extensive time-series analysis was performed to determine the statistical properties of the X-ray and the VLF wave data and the relationship between the two phenomena. The power spectral density functions of the > 5 keV and > 50 keV data were computed for the period 1148:00 to 1156:32 using 0.125 s bins to search for low-frequency periodicities in the data. The spectra appear to be identical within limits allowed by statistical variations in the spectral estimates. One may therefore conclude that if primary precipitating electrons of energies between 5 keV and 50 keV did contribute to the microbursts, their temporal variation was similar to those of energies above 50 keV. The shape of the spectrum of the X-ray data closely follows the function f^{-n} where n = 1.2. A broad low-amplitude peak was present at f = 1.5 Hz. This frequency corresponds to the periodicity of pulses within microburst groups. The X-ray power spectra were computed for 30 s intervals to look for interesting time variations in the character of the event and to examine the high-frequency spectral content. At the start of the microburst event the spectrum of the X-rays was enhanced by approximately two orders of magnitude over background at low frequencies. The power spectrum decreased rapidly at frequencies beyond 5 Hz. This cutoff frequency corresponds to the average width of the microburst being about 0.2 ± 0.2 seconds. The spectra were significantly reduced in amplitude around 1151:30 UT and 1153:20 UT. During these two intervals there was a noticeable reduction in the occurrence of microbursts.

Because the interaction of the energetic electrons and VLF waves depends crucially on the wave frequency, the time series analysis of the Roberval VLF data has been performed on three separate bands of frequency. The bands chosen covered the entire range of observed emissions: 1 - 2 kHz, 2 - 3 kHz and 3 - 4 kHz. The relatively coarse 1 kHz bandwidth was chosen to achieve a relative error of 20% for the spectral estimate of the power in these bands with a time resolution of 0.025 seconds (Bendat and Piersol, 1971).

17

The integrated VLF signal-strength data have much flatter power spectra than the X-rays. The estimated spectra are of the form $A(t) f^{-n}$ where $n = 0.4$, and $A(t)$ is a slowly varying amplitude modulation, believed to represent the group nature of the occurrence of the VLF emissions.

Since the variance of the data seems to be an important indicator of the VLF activity within a given interval, it has been plotted for the three bands of Roberval data along with the total variance of the > 5 keV X-ray data in Figure 6. The top panel displays the X-ray variance in units of thousands of counts s^{-1} cm^{-2} sr^{-1}. The other three panels show the variance of the VLF intensity in each of the three bands in arbitrary but equivalent units. The slow decrease in the X-ray microburst activity and the quiet periods at 1151:30 and 1153:20 are clearly visible. In contrast, the VLF data show a general increase during the ten minute period analyzed and there are significant differences in the three VLF frequency bands. The activity in the $1 - 2$ kHz band is at a maximum in the middle of the 10-minute period. With the aid of the VLF spectrograms this maximum is interpreted as a gradual dip of the low-band edge of the riser emissions. Some of the variations in the other bands may also be considered as changes in the average riser frequencies. However, the shifts seem to occur at different times for the high-frequency band than for the low-frequency band.

Figure 7 presents the coherence function surface of the > 5 keV X-ray data and the 2-3 kHz Roberval VLF intensity as a function of frequency and Universal Time. The data were analyzed in consecutive non-overlapping 25.6 s intervals using 25 ms averages, so that each interval consisted of 1024 points, and the frequency range of the resulting spectra was $0 - 20$ Hz. The full length of the microburst event was analyzed (1147 UT - 1157 UT). Individual coherence spectra were averaged in frequency over 32 points, so that each function has sixteen points, equally spaced over the frequency range. The value of the coherence at any point represents the fraction of the power in the X-ray data that was linearly related to the VLF data at that frequency and time. The minimum statistically significant coherence is approximately $0.2. - 0.3$, due to the amount of averaging performed in the analysis. Of the three VLF frequency bands studied, the 2-3 kHz band correlated most strongly

18
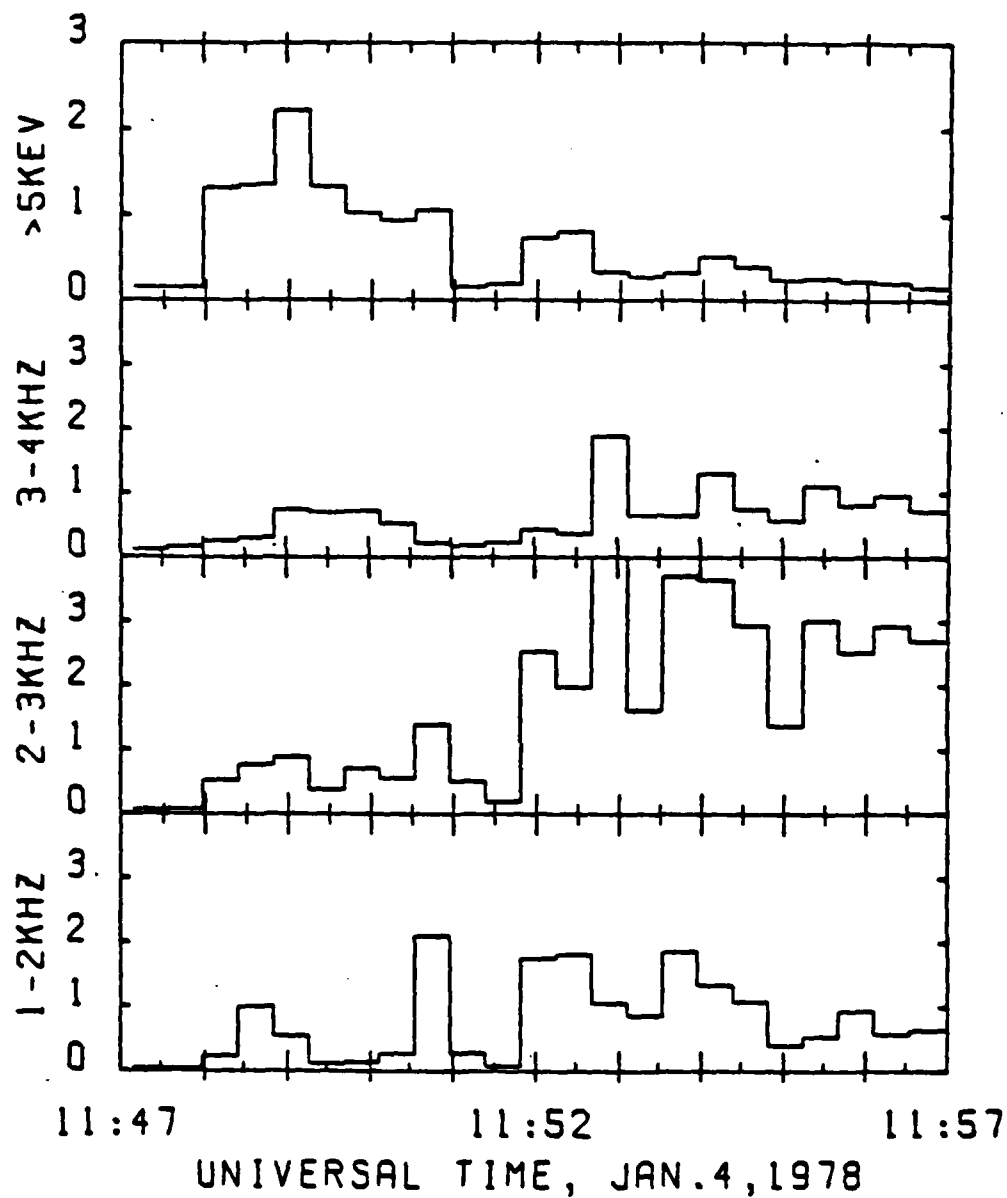
Fig. 6. Total variance of the >5 keV X-ray flux and the Roberval VLF inten-
sity in three frequency bands.

19

SUPER ARCAS 15.162UE COHERENCE SPECTRA
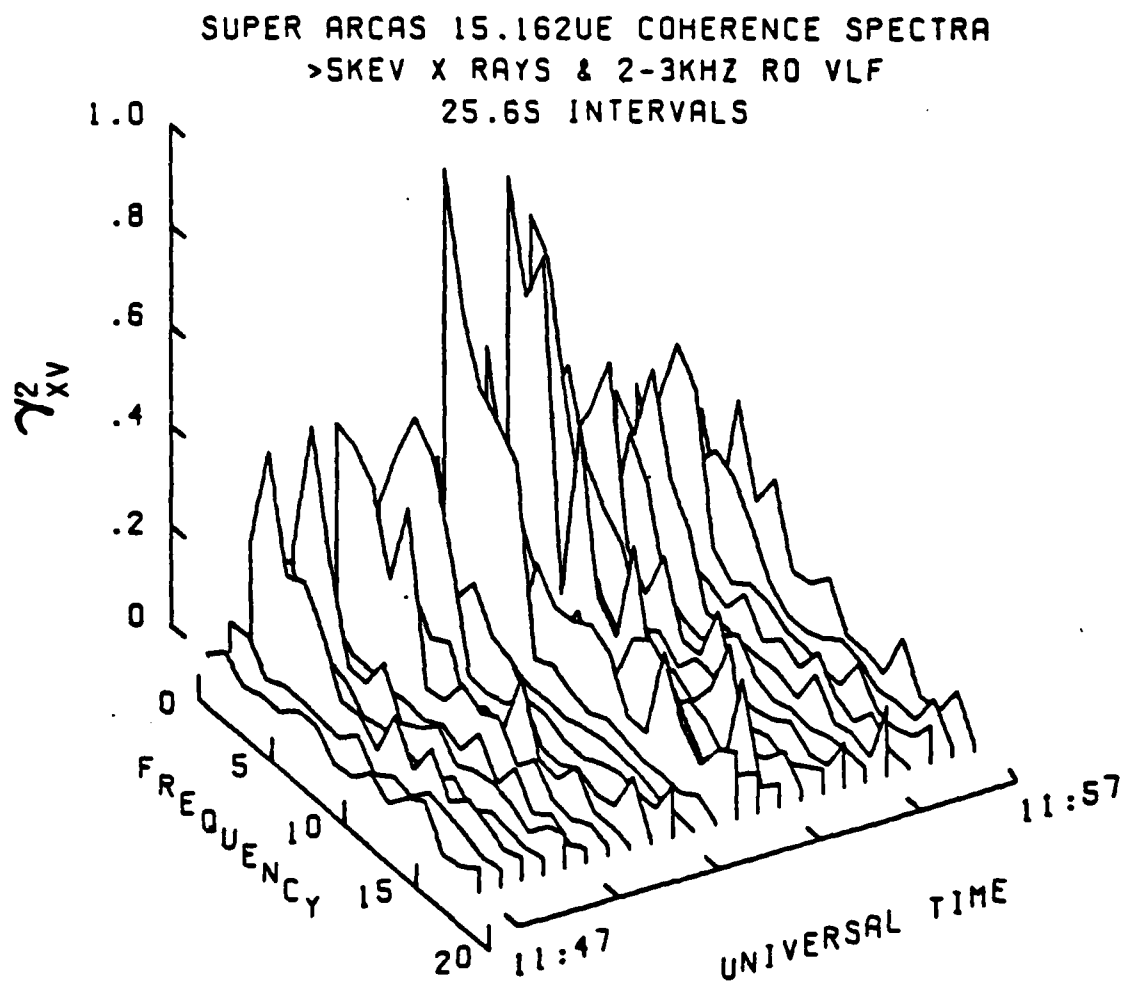>5KEV X RAYS & 2-3KHZ RO VLF
25.6S INTERVALS

Fig. 7. Coherence spectra of the >5 keV X-ray flux and the 2 - 3 kHz Roberval VLF intensity.

with the precipitation data. The coherence surface exhibits significant peaks throughout the event and a large enhancement during the time period mentioned previously (1151 - 1154 UT). The magnitude of the coherence of the 2 - 3 kHz VLF with the X-ray data during the interval approached the theoretical limit of unity at low frequencies.

To clarify the relative timing of the correlations of the X-rays and the VLF, the peak coherence is shown as a function of Universal Time in Figure 8. In this graph the maximum coherence was plotted without regard to its frequency. The three panels contain the peak coherence of the > 5 keV and the Roberval VLF signal. The enhancements of the 1 - 2 kHz and the 2 - 3 kHz coherence functions in the middle of the event are clearly evident in the figure. The decrease in the 3 - 4 kHz coherence is less pronounced, and seems to precede the increase in lower bands by more than a minute. If the changes of the peak coherences are compared with the variances of the data shown in Figure 6, intervals may be discerned in which the VLF data contained a large amount of power unrelated to the X-ray flux. For example, in the interval 1153:07.2 - 1153:32.8 UT, the coherence for the 1 - 2 kHz band had the value of 0.73, while the variance of the intensity of the 1 - 2 kHz band was 0.86. In the following interval, from 1153:32.8 to 1153:58.4 UT, the variance of the VLF intensity doubled to 1.87, while the coherence decreased to 0.36. The variance of the > 5 keV X-ray flux was approximately equal during the two intervals. Therefore, the decrease in coherence may be interpreted as an increase in the power of unrelated chorus emissions in the Roberval VLF data. However, this approach does not explain all the features of the coherence plots. In the interval 1148:25.6 - 1148:51.2 UT the coherence of the 2 - 3 kHz band decreased to half the value in the previous 25 seconds, but the variance of the > 5 keV X-rays and the 2 - 3 kHz Roberval VLF remains approximately equal in the two time intervals. Thus, the total power in the two time series was constant, but the fraction of related power in the data changed by a factor of 2. One possible explanation of this result is that there is a nonlinear relationship between electron precipitation and VLF intensities.

A correlation function analysis was used to determine the time delay between various correlated features in the X-ray fluxes and the Roberval VLF
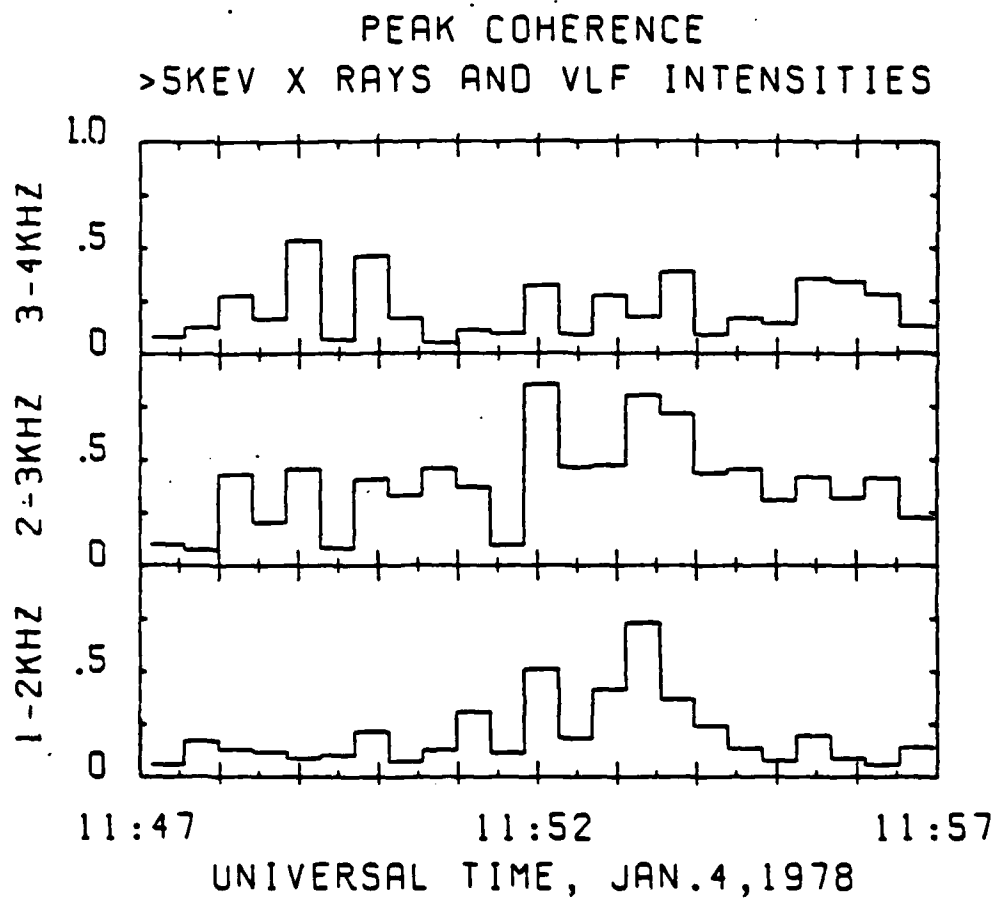
21

Fig. 8. Peak coherence of the >5 keV X-ray flux and the Roberval VLF intensities in three frequency bands.

data. Figure 9 presents the autocorrelation functions of the 2 - 3 kHz Roberval VLF intensity and the > 5 keV X-ray flux, and the crosscorrelation function of the X-rays and the VLF. The correlation functions were calculated using the standard convolution technique from 12.5 seconds of data in 25 ms averages, and plotted for the range of time lags -2 to 2 s. This figure was typical of the ones computed from data throughout the duration of the micro-burst event. Notable features include the large peak at zero time lag in the autocorrelation function of the VLF in the top panel of the figure. This indicates a large portion of power in the high frequencies (above 5 Hz). The smaller peaks at 0.59 s, 0.78 s, and 1.35 s suggest the presence of weak periodic components at those periods. The autocorrelation function of the X-ray flux is presented in the middle panel of the figure. The large random (nonperiodic) component in the data tends to broaden the peaks in the correlation function, which are located at time lags of 0.7 and 1.3 s. The central peak in the crosscorrelation function of the X-rays and the VLF data was of magnitude 0.68, indicating a significant correlation between the X-rays and the VLF at a small time delay. The best estimate of the delay was calculated from the centroid of the peak to be 0.016 s ± 0.08 s. The entire ten minutes of data during the microburst-chorus event were analyzed in 12.5 s intervals using the above techniques. The maximums of the crosscorrelation functions that were found ranged in value from 0.3 to 0.72, the larger values occurring during the periods for which the value of the coherence was above 0.3. The arrival time delay is defined by $T_{ew} = T_e - T_w$, where T_e is the arrival time of the electron precipitation at Siple, and T_w is the arrival time of the VLF emission at Roberval. The time delays of maximum correlation of the X-rays and the Roberval VLF data were small ($-0.05 < T_{ew} < 0.02$), with the X-rays usually arriving first. The uncertainty in the delay, due to the random nature of the data, is estimated to be approximately 0.08 - 0.1 s.

SUPER ARCAS 15.162UE CORRELATION FUNCTIONS
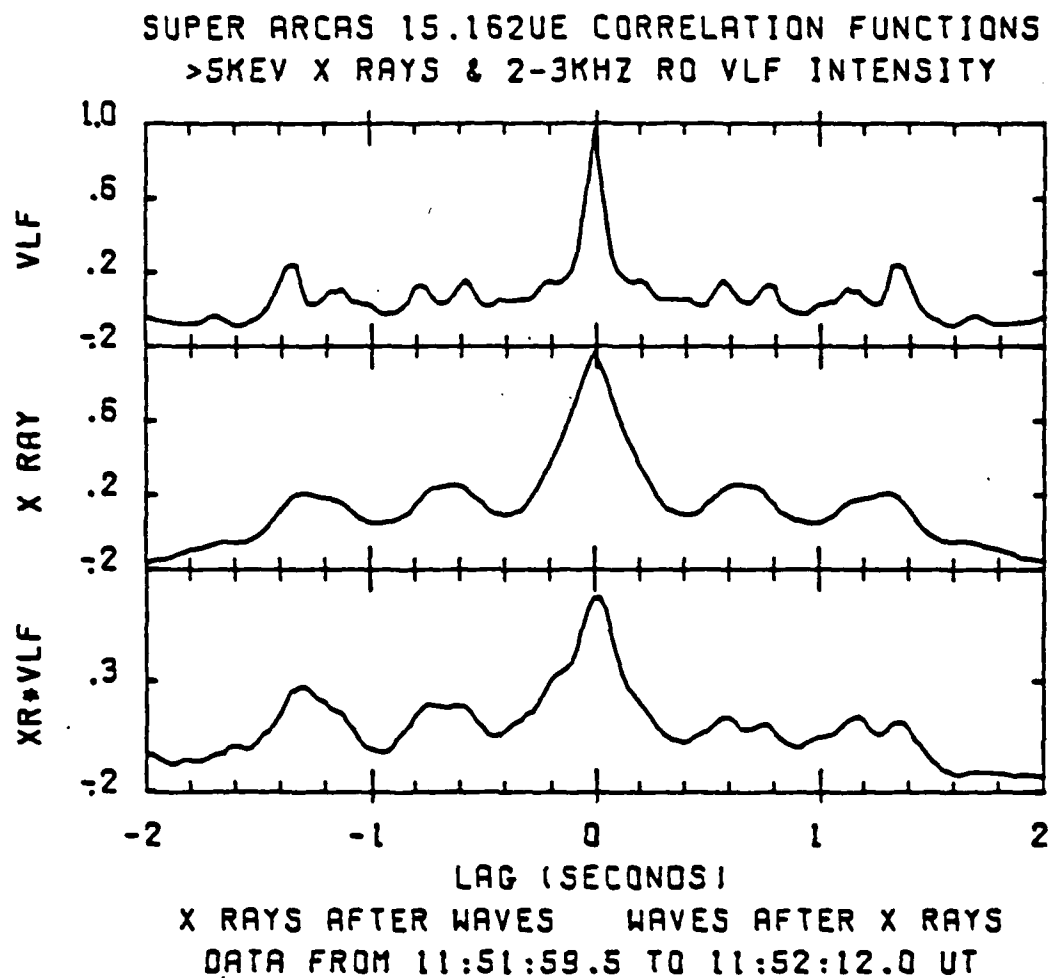>5KEV X RAYS & 2-3KHZ RO VLF INTENSITY

Fig. 9. Correlation functions of the >5 keV X-ray flux and 2 - 3 kHz Roberval
VLF intensity plotted versus time lag. The top and middle panels
present the autocorrelation functions of the observations, and the
bottom panel displays the crosscorrelation function.

24

IV. CONCLUSIONS

The data presented from this microburst event clearly indicate the very complex nature of the problem of relating VLF chorus emissions and electron precipitation. Even during a relatively brief observing time period (compared to that of a balloon payload), the character of the event changed dramatically. The obvious lack of detailed time correlations between chorus emissions and electron bursts is probably the outstanding feature of our data. This important aspect of such events has tended to get lost as experimenters have searched for and published only those few brief periods of high correlation that permit simpler analysis and explanation.

The observed time lags that we report are comparable to those reported by others from similar experiments on the Siple-Roberval field line. The small differences can easily be accounted for by variation in the equatorial cold plasma density and/or the location of the interaction region. Since no whistlers were observed during the period of interest from either Siple or Roberval, it has not been possible to explore this aspect of the interpretation of our data.

REFERENCES

Anderson, K. A., and D. W. Milton, "Balloon Observations of X-Rays in the Auroral Zone, 3. High-Time Resolution Studies," J. Geophys. Res., 69, 4457-4479 (1964).

Benbrook, J. R., E. A. Bering, III, H. Leverenz, J. L. Roeder, and W. R. Sheldon, "Quiet-Time Electron Precipitation at L = 4 in the South Atlantic Anomaly," J. Geophys. Res., 88, 189-199 (1983).

Bendat, Julius S., and Allen G. Piersol, Random Data: Analysis and Measurement Procedures, Wiley-Interscience, New York (1971).

Bering, E. A., J. R. Benbrook, E. G. Stansberry, W. R. Sheldon, and J. L. Roeder, "The Results From the X-ray Bremsstrahlung Experiment of Project Trigger," J. Geophys. Res., 85, 5079-5095 (1980).

Carpenter, D. L., J. C. Foster, T. J. Rosenberg, and L. J. Lanzerotti, "A Subauroral and Mid-Latitude View of Substorm Activity," J. Geophys. Res., 80, 4279-4286 (1975).

Chang, H. C., and U. S. Inan, "Quasi-Relativistic Electron Precipitation Due to Interactions with Coherent VLF Waves in the Magnetosphere," J. Geophys. Res., 88, 318-328 (1983).

Foster, J. C., and T. J. Rosenberg, "Electron Precipitation of VLF Emissions Associated with Cyclotron Resonance Interactions Near the Plasmapause," J. Geophys. Res., 81, 2183-2192 (1976).

Foster, J. C., T. J. Rosenberg, and L. J. Lanzerotti, "Magnetospheric Conditions at the Time of Enhanced Wave-Particle Interactions Near the Plasmapause," J. Geophys. Res., 80, 2175-2182 (1976).

Haugstad, Bjarne S., and Thorbjorn Pytte, "Effects of Primary Electron Transit Times on Power Spectra of Auroral-Zone X-ray Microbursts," J. Atmos. Terr. Phys., 39, 689-698 (1977).

Helliwell, R. A., S. B. Mende, J. H. Doolittle, W. C. Armstrong, and D. L. Carpenter, "Correlations Between λ 4278 Optical Emissions and VLF Wave Events Observed at L ~ 4 in the Antarctic," J. Geophys. Res., 85, 3376-3386 (1980).

Inan, U. S., T. F. Bell, and H. C. Chang, "Particle Precipitation Induced by Short-Duration VLF Waves in the Magnetosphere," J. Geophys. Res., 87, 6243-6264 (1982).

Inan, U. S., H. C. Chang, and R. A. Helliwell, "Electron Precipitation Zones Around Major Ground-Based VLF Signal Sources," J. Geophys. Res., 89, 2891-2906 (1984).

Lampton, M., "Daytime Observations of Energetic Auroral-Zone Electrons," J. Geophys. Res., 72, 5817-5823 (1967).

Oliven, M. N., and D. A. Gurnett, "Microburst Phenomena, 3. An Association Between Microbursts and VLF Chorus," J. Geophys. Res., 73, 2355-2362 (1968).

Oliven, M. N., D. Venkatesan, and K. G. McCracken, "Microburst Phenomena, 2. Auroral Zone Electrons," J. Geophys. Res., 73, 2345-2353 (1968).

Parks, G. K., "Auroral Zone Microbursts, Substructures, and a Model for Microburst Precipitation," Proc. Int. Conf. X-rays Space (Cosmic, Sol. Auroral X-ray), 2, 849-874 (1975).

Parks, G. K., "Microburst Precipitation Phenomena," J. Geomag. Geoelectr., 30, 327-341 (1978).

Roeder, J. L., W. R. Sheldon, J. R. Benbrook, E. A. Bering, and H. Leverenz, "X-ray Measurements During the ARAKS Experiments," Ann. Geophys., 36, 401-409 (1980).

Rosenberg, T. J., R. A. Helliwell, and J. P. Katsufrakis, "Electron Precipitation Associated with Discrete Very Low Frequency Emissions," J. Geophys. Res., 76, 8445-8452 (1971).

Rosenberg, T. J., K. Marthinsen, J. A. Holtet, A. Egeland, and D. L. Carpenter, "Evidence of the Common Origin of Electron Microbursts and VLF Chorus," J. Geomag. Geoelectr., 30, 355-356 (1978).

Rosenberg, T. J., J. C. Siren, D. L. Matthews, K. Marthinsen, J. A. Holtet, A. Egeland, D. L. Carpenter, and R. A. Helliwell, "Conjugacy of Electron Microbursts and VLF Chorus," J. Geophys. Res., 86, 5819-5832 (1981).

LABORATORY OPERATIONS

The Laboratory Operations of The Aerospace Corporation is conducting experimental and theoretical investigations necessary for the evaluation and application of scientific advances to new military space systems. Versatility and flexibility have been developed to a high degree by the laboratory personnel in dealing with the many problems encountered in the nation's rapidly developing space systems. Expertise in the latest scientific developments is vital to the accomplishment of tasks related to these problems. The laboratories that contribute to this research are:

Aerophysics Laboratory: Launch vehicle and reentry fluid mechanics, heat transfer and flight dynamics; chemical and electric propulsion, propellant chemistry, environmental hazards, trace detection; spacecraft structural mechanics, contamination, thermal and structural control; high temperature thermomechanics, gas kinetics and radiation; cw and pulsed laser development including chemical kinetics, spectroscopy, optical resonators, beam control, atmospheric propagation, laser effects and countermeasures.

Chemistry and Physics Laboratory: Atmospheric chemical reactions, atmospheric optics, light scattering, state-specific chemical reactions and radiation transport in rocket plumes, applied laser spectroscopy, laser chemistry, laser optoelectronics, solar cell physics, battery electrochemistry, space vacuum and radiation effects on materials, lubrication and surface phenomena, thermionic emission, photosensitive materials and detectors, atomic frequency standards, and environmental chemistry.

Computer Science Laboratory: Program verification, program translation, performance-sensitive system design, distributed architectures for spaceborne computers, fault-tolerant computer systems, artificial intelligence and microelectronics applications.

Electronics Research Laboratory: Microelectronics, GaAs low noise and power devices, semiconductor lasers, electromagnetic and optical propagation phenomena, quantum electronics, laser communications, lidar, and electro-optics; communication sciences, applied electronics, semiconductor crystal and device physics, radiometric imaging; millimeter wave, microwave technology, and RF systems research.

Materials Sciences Laboratory: Development of new materials: metal matrix composites, polymers, and new forms of carbon; nondestructive evaluation, component failure analysis and reliability; fracture mechanics and stress corrosion; analysis and evaluation of materials at cryogenic and elevated temperatures as well as in space and enemy-induced environments.

Space Sciences Laboratory: Magnetospheric, auroral and cosmic ray physics, wave-particle interactions, magnetospheric plasma waves; atmospheric and ionospheric physics, density and composition of the upper atmosphere, remote sensing using atmospheric radiation; solar physics, infrared astronomy, infrared signature analysis; effects of solar activity, magnetic storms and nuclear explosions on the earth's atmosphere, ionosphere and magnetosphere; effects of electromagnetic and particulate radiations on space systems; space instrumentation.

. . .

LABORATORY OPERATIONS

The Laboratory Operations of The Aerospace Corporation is conducting experimental and theoretical investigations necessary for the evaluation and application of scientific advances to new military space systems. Versatility and flexibility have been developed to a high degree by the laboratory personnel in dealing with the many problems encountered in the nation's rapidly developing space systems. Expertise in the latest scientific developments is vital to the accomplishment of tasks related to these problems. The laboratories that contribute to this research are:

Aerophysics Laboratory: Launch vehicle and reentry fluid mechanics, heat transfer and flight dynamics; chemical and electric propulsion, propellant chemistry, environmental hazards, trace detection; spacecraft structural mechanics, contamination, thermal and structural control; high temperature thermomechanics, gas kinetics and radiation; cw and pulsed laser development including chemical kinetics, spectroscopy, optical resonators, beam control, atmospheric propagation, laser effects and countermeasures.

Chemistry and Physics Laboratory: Atmospheric chemical reactions, atmospheric optics, light scattering, state-specific chemical reactions and radiation transport in rocket plumes, applied laser spectroscopy, laser chemistry, laser optoelectronics, solar cell physics, battery electrochemistry, space vacuum and radiation effects on materials, lubrication and surface phenomena, thermionic emission, photosensitive materials and detectors, atomic frequency standards, and environmental chemistry.

Computer Science Laboratory: Program verification, program translation, performance-sensitive system design, distributed architectures for spaceborne computers, fault-tolerant computer systems, artificial intelligence and microelectronics applications.

Electronics Research Laboratory: Microelectronics, GaAs low noise and power devices, semiconductor lasers, electromagnetic and optical propagation phenomena, quantum electronics, laser communications, lidar, and electrooptics; communication sciences, applied electronics, semiconductor crystal and device physics, radiometric imaging; millimeter wave, microwave technology, and RF systems research.

Materials Sciences Laboratory: Development of new materials: metal matrix composites, polymers, and new forms of carbon; nondestructive evaluation, component failure analysis and reliability; fracture mechanics and stress corrosion; analysis and evaluation of materials at cryogenic and elevated temperatures as well as in space and enemy-induced environments.

Space Sciences Laboratory: Magnetospheric, auroral and cosmic ray physics, wave-particle interactions, magnetospheric plasma waves; atmospheric and ionospheric physics, density and composition of the upper atmosphere, remote sensing using atmospheric radiation; solar physics, infrared astronomy, infrared signature analysis; effects of solar activity, magnetic storms and nuclear explosions on the earth's atmosphere, ionosphere and magnetosphere; effects of electromagnetic and particulate radiations on space systems; space instrumentation.

. . .